Supporting Information

Confined pyrolysis of a dye pollutant for two-dimensional F,N,S tri-doped nanocarbon as a high performance oxidative coupling reaction catalyst

Sijie Liu[a], Sian Chen[b], Ao Yu[a], Yajing Hu[a], Bingzhe Yu[a], Haining Wang[b], Ping Peng[a,] and Fang-Fang Li[a,]**

[a] State Key Laboratory of Materials Processing and Die & Mould Technology, School of Materials Science and Engineering, Huazhong University of Science and Technology, Wuhan 430074, China.
[b] Beijing Key Laboratory of Bio-inspired Energy Materials and Devices, School of Space and Environment, Beihang University, Beijing 100191, China.

Corresponding Author

*E-mail: ppeng@hust.edu.cn; ffli@hust.edu.cn

Table of contents

Fig. S1. Digital images of Mg-Al LDH, Mg-Al LDO, AR337-LDH and FNSHC.

Fig. S2. Chemical structure of acid red-337 (AR-337). The estimated molecular size of the dye anion was 13 Å × 7 Å × 3 Å in three dimensions.

Fig. S3. Chemical structures of methyl red sodium salt (a), sodium *p*-toluenesulfonate (b) and methyl orange (c).

Fig. S4. SEM images of Mg-Al LDH (a), Mg-Al LDO (b), AR337-LDH (c), FNSHC-600 (d), FSNHC-650 (e), FNSHC-700 (f), FNSHC-750 (g) and FNSHC-800 (h). Scale bar, 500 nm.

Fig. S5. PXRD patterns of Mg-Al LDH (a) and Mg-Al LDO (b).

Fig. S6. PXRD patterns of Mg-Al LDH, AR-337 and AR337-LDH.

Fig. S7. Morphology of FNSHC-700. (a) Low magnification SEM image. (b) High magnification SEM image. (**c**) High magnification TEM image.

Fig. S8. SEM images of FNSC-700.

Fig. S9. PXRD patterns of FNSC-700, FNSHC-600, FNSHC-700 and FNSHC-800.

Fig. S10. N_2 adsorption/desorption isotherms and pore size distribution curve of FNSC-700.

Fig. S11. N_2 adsorption/desorption isotherms and pore size distribution curve of FNSHC-600.

Fig. S12. N_2 adsorption/desorption isotherms and pore size distribution curve of FNSHC-700.

Fig. S13. N_2 adsorption/desorption isotherms and pore size distribution curve of FNSHC-800.

Table S1. XPS analytic data of FNSC-700, FNSHC-600, FNSHC-650, FNSHC-700, FNSHC-750, FNSHC-800 and FNSHC-700-R.

Fig. S14. High resolution XPS spectra of C 1s of FNSC-700 (**a**), FNSHC-600 (**b**), FNSHC-700 (c) and FNSHC-800 (**d**).

Fig. S15. High resolution XPS spectra of C 1s (a), N 1s (b), S 2p (c) and F 1s (d) of FNSHC-700-R.

Table S2. Comparison of catalytic activities over FNSHC-700 and other carbocatalysts for the oxidative self-coupling of benzylamine.

Table S3. Comparison of catalytic activities over FNSHC-700 and heterogeneous metal-based catalyst for the oxidative self-coupling of benzylamine.

Table S4 Oxidation cross-coupling of benzylamine and 4-fluorobenzylamine over FNSHC-700 catalyst.

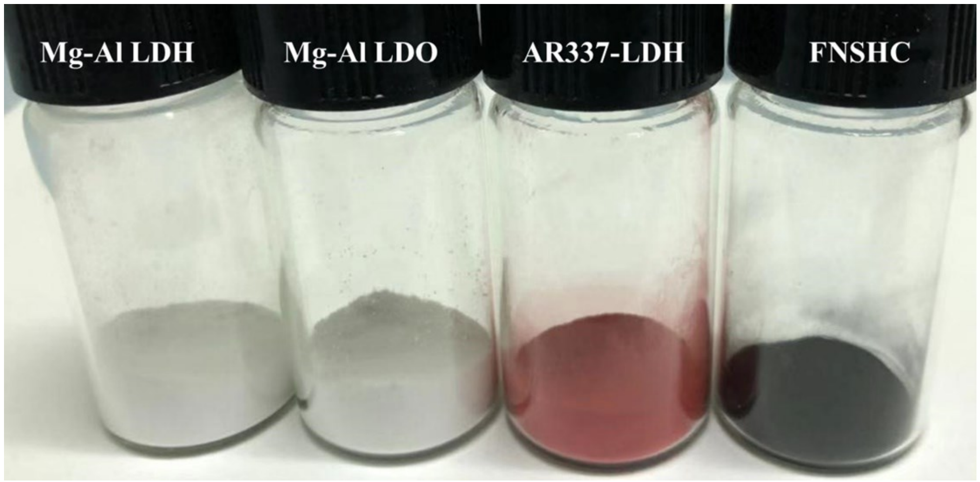

Fig. S1 Digital images of Mg-Al LDH, Mg-Al LDO, AR337-LDH and FNSHC.

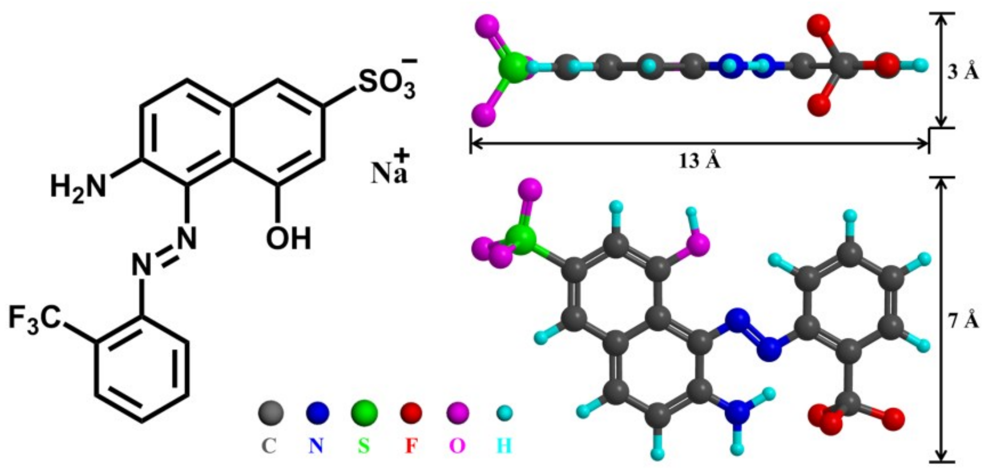

Fig. S2 Chemical structure of acid red-337 (AR-337). The estimated molecular size of the dye anion was 13 Å × 7 Å × 3 Å in three dimensions.

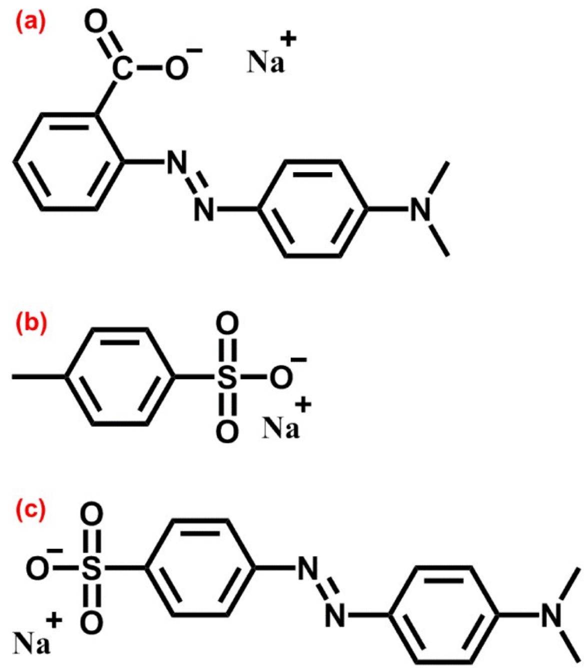

Fig. S3 Chemical structures of methyl red sodium salt (a), sodium *p*-toluenesulfonate (b) and methyl orange (c).

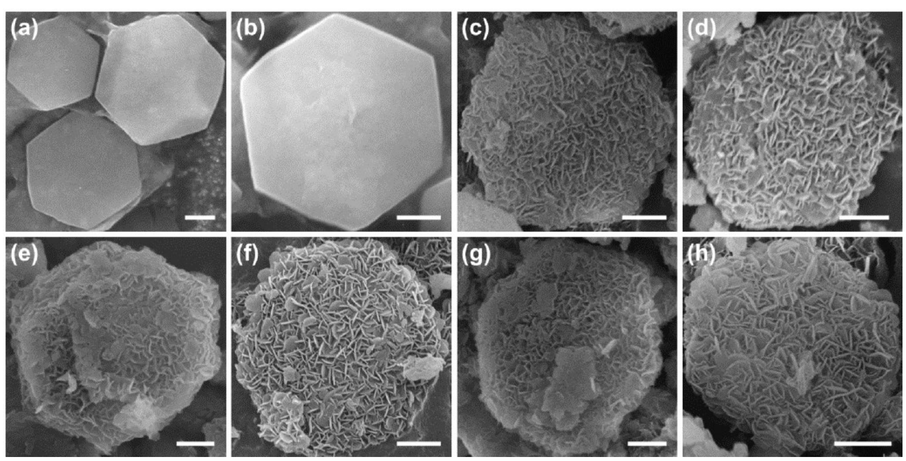

Fig. S4 SEM images of Mg-Al LDH (a), Mg-Al LDO (b), AR337-LDH (c), FNSHC-600 (d), FSNHC-650 (e), FNSHC-700 (f), FNSHC-750 (g) and FNSHC-800 (h). Scale bar, 500 nm.

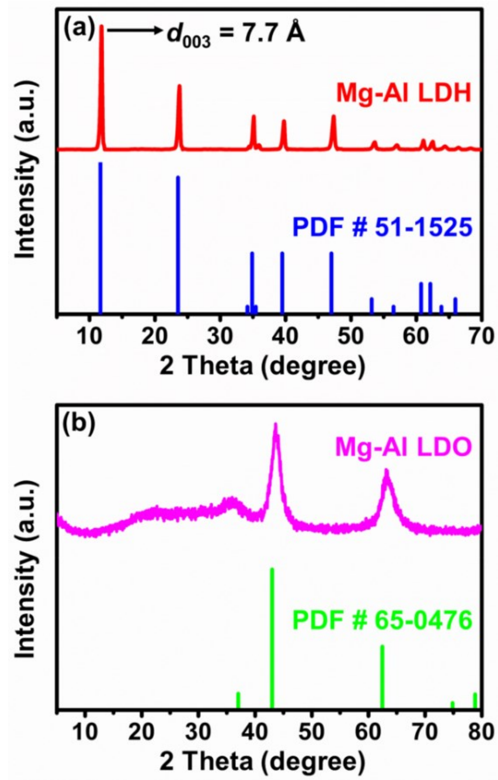

Fig. S5 PXRD patterns of Mg-Al LDH (a) and Mg-Al LDO (b).

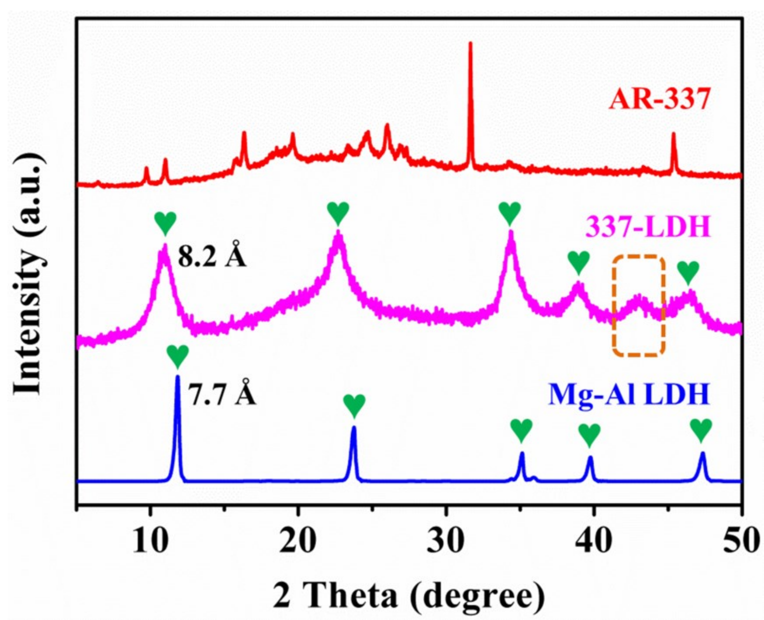

Fig. S6 PXRD patterns of Mg-Al LDH, AR-337 and AR337-LDH.

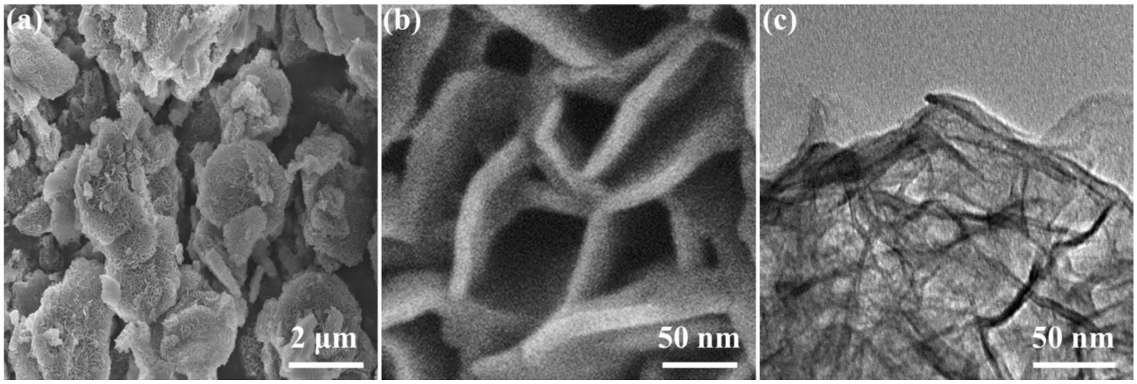

Fig. S7 Morphology of FNSHC-700. (a) Low magnification SEM image. (b) High magnification SEM image. (**c**) High magnification TEM image.

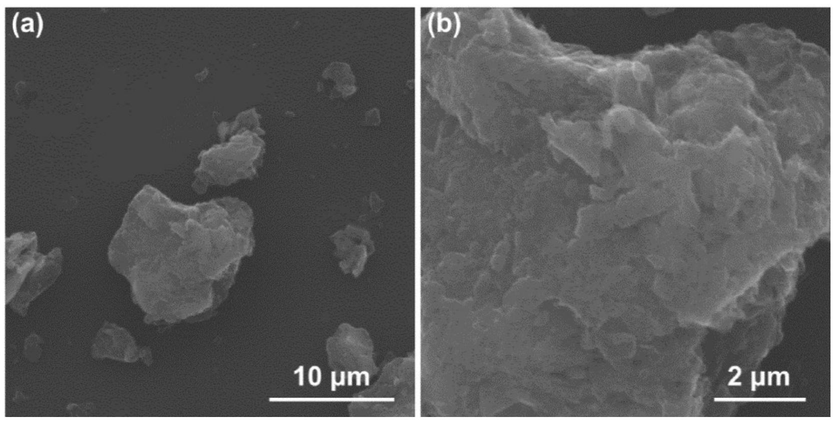

Fig. S8 SEM images of FNSC-700.

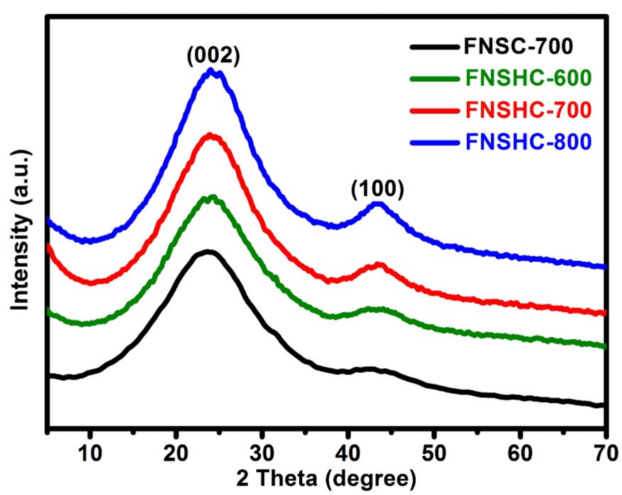

Fig. S9 PXRD patterns of FNSC-700, FNSHC-600, FNSHC-700 and FNSHC-800.

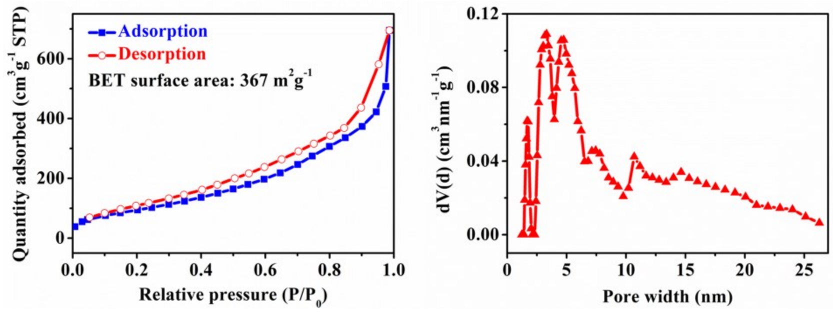

Fig. S10 N_2 adsorption/desorption isotherms and pore size distribution curve of FNSC-700.

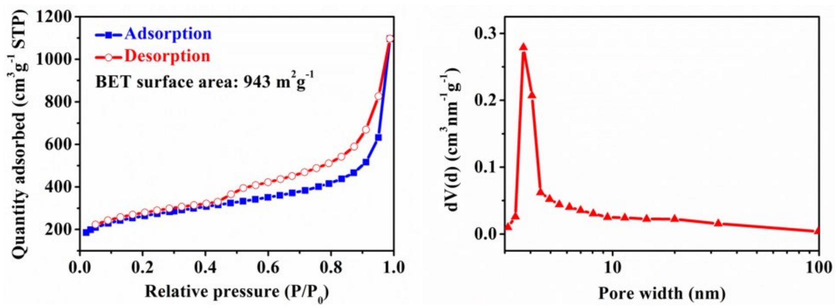

Fig. S11 N_2 adsorption/desorption isotherms and pore size distribution curve of FNSHC-600.

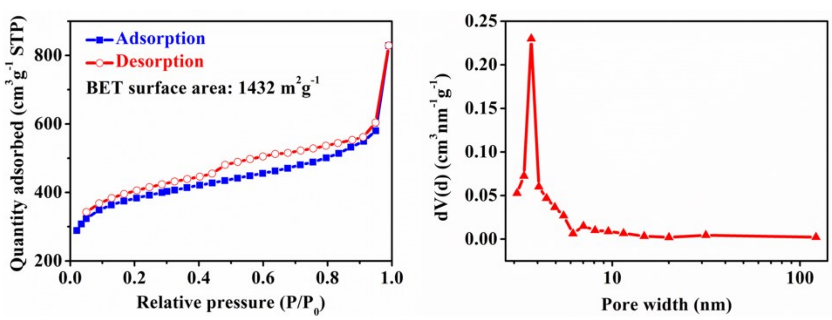

Fig. S12 N_2 adsorption/desorption isotherms and pore size distribution curve of FNSHC-700.

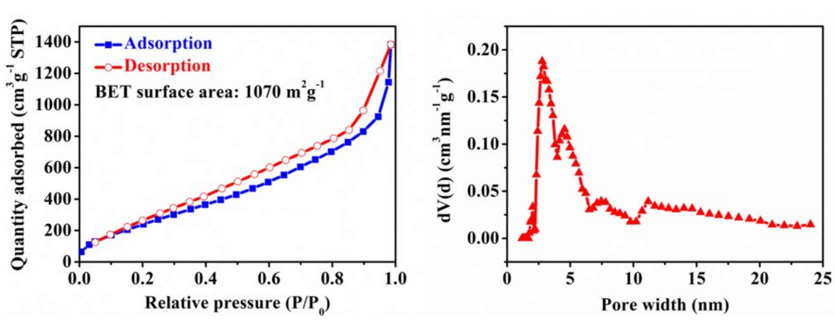

Fig. S13 N_2 adsorption/desorption isotherms and pore size distribution curve of FNSHC-800.

Table S1 XPS analytic data of FNSC-700, FNSHC-600, FNSHC-700, FNSHC-800 and FNSHC-700-R

Sample	C (at%)	F (at%)	N (at%)	S (at%)	O (at%)
FNSC-700	87.05	0.12	4.54	1.71	6.58
FNSHC-600	82.07	3.42	7.21	1.63	5.67
FNSHC-650	83.66	2.91	5.46	1.28	6.69
FNSHC-700	85.57	2.43	3.93	0.67	7.40
FNSHC-750	85.92	1.88	3.53	1.05	7.62
FNSHC-800	86.71	1.33	3.07	1.34	7.55
FNSHC-700-R	85.57	2.18	4.12	0.71	7.42

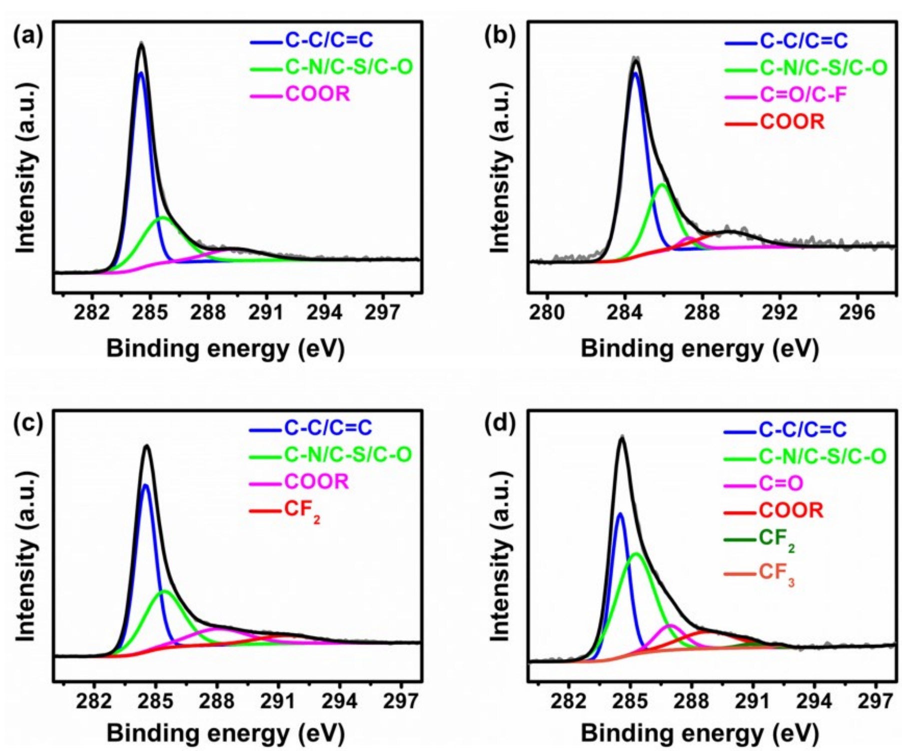

Fig. S14 High resolution XPS spectra of C 1s of FNSC-700 (**a**), FNSHC-600 (**b**), FNSHC-700 (c) and FNSHC-800 (**d**).

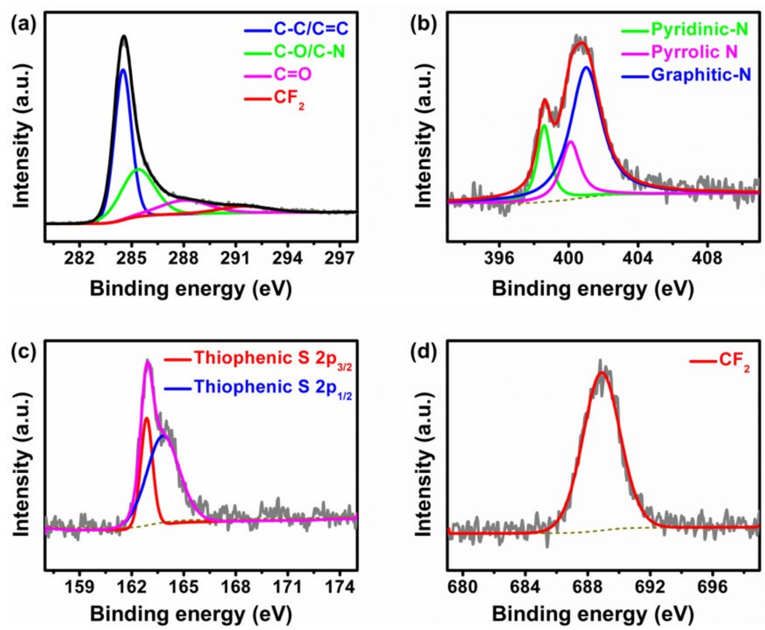

Fig. S15 High resolution XPS spectra of C 1s (a), N 1s (b), S 2p (c) and F 1s (d) of the catalyst (FNSHC-700-R) after 10 cycling tests.

Table S2 Comparison of catalytic activities over FNSHC-700 and other carbocatalysts for the oxidative self-coupling of benzylamine[a]

Catalyst	n_1 (mmol)	Catalyst loading (wt%)	n_2 (mmol)	T (°C)	Atmosphere	t (h)	TOF (h^{-1})	SSA (m^2g^{-1})	Ref.
FNSHC-700	**4.57**	**2**	**0.83**	**85**	**Air**	**4**	**1.38**	**1432**	**This work**
B,N co-doped holey graphene	0.91	28	2.50	85	O_2	4	0.09	978	[14]
Modified graphene oxide	9.15	5	4.17	90	Air	12	0.18	365	[13]
Mesoporous carbon	4.71	3.7	1.67	100	O_2	5.5	0.51	751	[16]
Nanoporous carbons derived from MOFs	5.00	3.7	1.67	100	O_2	12	0.25	362	[18]
Graphite oxide	4.90	50	22.32	100	O_2 (5 atom)	4	0.05	69	[12]
N-doped carbon nanosheets	1.00	14.00	1.25	120	Air	8	0.10	594	[23]
P-doped nanomesh graphene	0.38	10	0.38	100	O_2	12	0.08	1414	[27]
B-doped mesoporous carbon	2.70	3.11	0.83	100	O_2	14	0.23	856	[25]
B,N co-doped graphene/ carbon nanotubes	0.92	28	2.50	85	O_2	3	0.12	398	[15]
Mesoporous carbon	4.35	3.7	1.67	100	O_2	8	0.33	637	[17]
N,O-doped mesoporous carbons	0.39	112	5	110	O_2 (5 atom)	4	0.02	656	[26]
Oxygen-rich carbon quantum dots	5.72	4	2.08	90	O_2	12	0.23	--	[24]
Triazine decorated graphene	0.46	75	3.33	60	O_2	24	0.006	778	[21]
Porous N-doped carbon	19.21	14	25	110	Air	14	0.05	591	[22]
N-doped hierarchically porous carbon	5.00	3.7	1.67	100	O_2	24	0.12	1536	[20]
Hierarchically porous carbon nanosheets	5.00	3.7	1.67	100	Air	13	0.23	1318	[19]

[a] n_1 represents the amount of benzylamine converted into imine, n_2 represents the amount of catalyst, t represents the reaction time. TOF = $n_1/(n_2*t)$.

Table S3 Comparison of catalytic activities over FNSHC-700 and heterogeneous metal-based catalyst for the oxidative self-coupling of benzylamine[a]

Catalyst	n_1 (mmol)	Catalyst loading (wt%)	n_2 (mmol)	T (°C)	Atmosphere	t (h)	TOF (h^{-1})	SSA (m^2g^{-1})	Ref.
FNSHC-700	**4.57**	**2**	**0.83**	**85**	**Air**	**4**	**1.38**	**1432**	**This work**
Acetylacetone - modified MnO_x	0.906	--	0.1	90	O_2 (3 atom)	14	0.65	--	[11]
Mesoporous copper aluminum mixed metal oxides	3	31	0.55	100	Air	15	0.36	140	[10]
Meso Cs/MnO_x	0.5	47	0.15	110	Air	3	1.11	79	[9]
MOF-253	10	--	0.15	100	Air	24	2.78	--	[8]
Au powder	0.112	4666	5.08	100	O_2	24	0.001	0.35	[7]

[a] n_1 represents the amount of benzylamine converted into imine, n_2 represents the amount of catalyst, t represents the reaction time. TOF = $n_1/(n_2*t)$.

Table S4 Oxidation cross-coupling of benzylamine and 4-fluorobenzylamine over FNSHC-700 catalyst[a]

Entry	Substrate 1	Substrate 2	Molar Ratio[b]	Product 3	Conversion (%)[c]	Selectivity (%)[d]
1	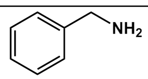	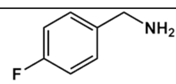	1/1	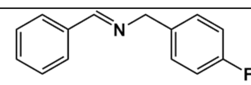	99	37
2	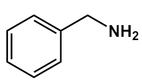	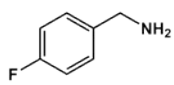	1/3	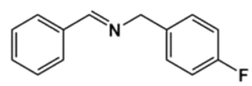	99	43

[a] Reaction conditions: benzylamine (0.5 g), catalyst (2 wt% catalyst loading), CH_3CN, 85 °C, open air, 12 h.

[b] Molar ratio of Substrate 1 and Substrate 2.

[c] Conversion was calculated based on substrate 1.

[d] Selectivity was calculated based on products 3.